Received: 29 July 2022 | Revised: 7 September 2022 | Accepted: 30 September 2022

DOI: 10.1002/cey2.308

RESEARCH ARTICLE

CARBON ENERGY WILEY

Long-lasting, reinforced electrical networking in a high-loading Li_2S cathode for high-performance lithium–sulfur batteries

Hun Kim[1] | **Kyeong-Jun Min**[1] | **Sangin Bang**[1] | **Jang-Yeon Hwang**[2] | **Jung Ho Kim**[3] | **Chong S. Yoon**[4] | **Yang-Kook Sun**[1,3]

[1]Department of Energy Engineering, Hanyang University, Seoul, Republic of Korea

[2]Department of Materials Science and Engineering, Chonnam National University, Gwangju, Republic of Korea

[3]Institute for Superconducting & Electronic Materials (ISEM), Australian Institute of Innovative Materials (AIIM), University of Wollongong, New South Wales, North Wollongong, Australia

[4]Department of Materials Science and Engineering, Hanyang University, Seoul, Republic of Korea

Correspondence
Yang-Kook Sun, Department of Energy Engineering, Hanyang University, Seoul 04763, Republic of Korea.
Email: yksun@hanyang.ac.kr

Funding information
Korea Institute of Energy Technology Evaluation and Planning, Grant/Award Number: 20214000000320; Samsung Research Funding & Incubation Center of Samsung Electronics, Grant/Award Number: SRFC-MA1901-06

Abstract

Realizing a lithium sulfide (Li_2S) cathode with both high energy density and a long lifespan requires an innovative cathode design that maximizes electrochemical performance and resists electrode deterioration. Herein, a high-loading Li_2S-based cathode with micrometric Li_2S particles composed of two-dimensional graphene (Gr) and one-dimensional carbon nanotubes (CNTs) in a compact geometry is developed, and the role of CNTs in stable cycling of high-capacity Li–S batteries is emphasized. In a dimensionally combined carbon matrix, CNTs embedded within the Gr sheets create robust and sustainable electron diffusion pathways while suppressing the passivation of the active carbon surface. As a unique point, during the first charging process, the proposed cathode is fully activated through the direct conversion of Li_2S into S_8 without inducing lithium polysulfide formation. The direct conversion of Li_2S into S_8 in the composite cathode is ubiquitously investigated using the combined study of in situ Raman spectroscopy, in situ optical microscopy, and cryogenic transmission electron microscopy. The composite cathode demonstrates unprecedented electrochemical properties even with a high Li_2S loading of 10 mg cm^{-2}; in particular, the practical and safe Li–S full cell coupled with a graphite anode shows ultra-long-term cycling stability over 800 cycles.

KEYWORDS

carbon nanotubes, electrical network, high energy, high loading, Li_2S cathode, lithium–sulfur batteries

1 | INTRODUCTION

Owing to the theoretical capacity limit and increasing cost of layered cathode materials, such as $LiCoO_2$, $Li(Ni_xCo_yMn_z)O_2$, and $Li(Ni_xCo_yAl_z)O_2$, next-generation batteries with a high energy density and low cost have attracted attention in the global energy storage market. Among them, rechargeable Li–S batteries using resource-abundant sulfur as an active material are now considered batteries that are closest to practical use.[1,2] Sulfur can theoretically offer a high capacity of 1675 mAh g^{-1}, and practically designed Li–S batteries are projected to achieve a high energy density between 400 and 500 Wh kg^{-1}.[3–5] Meanwhile, lithium sulfide (Li_2S)-based Li–S batteries have attracted considerable attention in recent years owing to the freedom of anode selection without being limited to the use of Li metal anode.[6,7] Unlike the general S-based Li–S batteries using S_8 as the cathode active material, Li_2S-based Li–S batteries contain a Li source at the cathode before cycling. Therefore, Li-free anodes, such as graphite, Si, and alloying composites, can be adopted, thus evading safety concerns and uncontrollable side reactions on the surface of metallic Li.[6–10]

To achieve the high energy density expected from Li–S batteries, it is essential to manufacture high-sulfur-loading electrodes with high sulfur contents that have high sulfur utilization. As the loading level of the electrode increases, however, the electrode inevitably thickens, thereby retarding electron transfer toward the whole electrode.[11,12] Uniform electron conduction across the electrode is crucial, especially in designing a high-energy Li_2S cathode that includes a higher content of insulating Li_2S and minimal amounts of conductive carbon materials. Numerous studies have been reported in the field of Li–S batteries using highly conductive graphene (Gr) and carbon nanotubes (CNTs) as conductive materials to effectively exchange electrons with sulfur and Li_2S.[13–19] However, although the excellent electrical properties of Gr and CNTs have been well demonstrated, the dimensional properties of each material and their role in Li–S batteries have been relatively less investigated. Gr and CNTs, which still have untapped potential, must be studied when applied to their respective applications.[20] The morphological properties of each carbon material and their interplay with the active material inside the electrode must also be carefully considered to better understand the function of each carbon material and thus to design high-energy, long-life Li_2S cathodes.

Apart from the common issue of Li–S batteries like lithium polysulfide (LiPs) dissolution, a major research area in Li_2S-based Li–S batteries is the initial activation of bulk Li_2S. Activation of this electrochemically insulating material (~10–13 S cm^{-1}) during the first delithiation process requires high activation energy,[21,22] and the initially activated Li_2S dominantly determines the energy density and cycling capacity of Li_2S-based Li–S batteries (Figure S1), which explains the importance of effectively activating Li_2S.[7,23–25] Meanwhile, a direct conversion reaction that oxidizes Li_2S to S_8, directly, without forming intermediate polysulfide, during the first activation process has been reported.[26–28] Manipulating the formation of LiPs is important because the dissolution of LiPs into the electrolyte is the underlying cause of the limited cycle life of Li–S batteries, as it induces the loss of active materials and initiates uncontrollable side reactions. Although a few studies have monitored the direct conversion mechanism of Li_2S, this area of research is still in its infancy.

Herein, we aim to fabricate a high-loading, high-energy, and long-life Li_2S cathode; thus, we prepare a rationally designed Gr/CNT composite and use this carbon matrix to fabricate a compact Li_2S/Gr/CNT cathode with a high Li_2S loading of up to 15 mg cm^{-2} using a simple pelletization method. An electrically well-connected network as well as the compact geometry of the proposed cathode effectively activates the Li_2S and enables reversible cycling by enhancing the electron transfer kinetics between the Li_2S and the carbon matrix. Finally, the unique activation process and the direct conversion reaction, occurring during the first charging process of the compact Li_2S/Gr/CNT cathode, is investigated using in situ techniques and cryo-transmission electron microscopy (TEM) analysis.

2 | EXPERIMENTAL SECTION

2.1 | Synthesis of the Gr/CNT composite

To prepare the Gr/CNT composite, Gr (1–5 atomic layer, ACROS) and multiwalled carbon nanotubes (MWCNTs, 95%; Nanolab) were separately dispersed in *N*-methyl-2-pyrrolidone (NMP; 99.50%; Daejung Chemicals & Metals) by ultrasonication for 30 min. Then, the Gr and MWCNT dispersions were combined at various mass ratios (7:1, 4:1, 1:1) and further ultrasonicated for 30 min. After vacuum filtration and washing with ethanol, the obtained Gr/CNT composites were dried in a vacuum oven (60°C) more than one day and then further dried in the same oven (190°C) overnight before use.

2.2 | Fabrication of the compact Li_2S/Gr/CNT cathode

Commercially available Li_2S powder (99.98%; Sigma-Aldrich), which was unsealed in an Ar-filled glovebox (water and oxygen content < 0.1 ppm), and the synthesized

Gr/CNT composites were homogeneously mixed via mechanical ball milling at a 75:25 mass ratio. The required amount of the Li_2S/Gr/CNT composite was pressed into a pellet mold (inner diameter of 10 mm) at 1 GPa for 5 min. Compact Li_2S/Gr/CNT cathodes with Li_2S loading levels of 10 or 15 mg cm^{-2} were thus obtained (the margin of error for the target loading was less than 0.1 mg cm^{-2}). To prepare the Li_2S/Gr and Li_2S/CNT cathodes, the Gr/CNT composite was replaced with Gr or CNTs in the ball-milling step with Li_2S. For the pouch-type cell, rectangular (30 mm × 50 mm) compact Li_2S/Gr/CNT cathodes with a Li_2S loading level of 10 mg cm^{-2} were prepared using the same fabrication process but with a rectangular pellet mold. All steps were performed in the Ar-filled glovebox (water and oxygen content < 0.1 ppm).

2.3 | Fabrication of the graphite anode

Graphite (POSCO Chem. Inc.), Super P (TIMCAL), and a polyacrylic acid binder (average Mv ~450,000; Sigma-Aldrich) were mixed in NMP at a mass ratio of 92:1:7, and the slurry was cast on a Cu foil. The prepared electrode was dried in a vacuum oven (60°C) more than one day and then further dried in the same vacuum oven at 110°C overnight before use. The capacity ratio of the anode to the cathode (N/P ratio) was set to 1.2:1.

2.4 | Fabrication of a pouch-type cell

For both electrodes, double-sided compact Li_2S/Gr/CNT cathodes (30 mm × 50 mm) and single-sided (31 mm × 51 mm) Li metal (200 μm; Hohsen Corp.) or as-prepared graphite anodes (31 mm × 51 mm) were used. For the separator, a polypropylene separator (Celgard 2400; Celgard) with 34 mm × 54 mm in size was used. An Al foil with an Al tap (cathode) and a Cu foil with a Ni tap (anode) were used as the current collectors. The pouch-type cell was fabricated using the winding method, and an Al-laminated film was used to package the cell. The electrolyte solutions (half-cell or full cell) and the ratio of the electrolyte and the active material content (Li_2S) for the pouch-type cell were the same as those of the coin-type cells.

2.5 | Electrochemical measurements

General half-cell tests were performed using a 2032 coin-type cell containing the prepared cathode (10 mm in diameter), a Li metal anode with a thickness of 200 μm (14 mm in diameter), and a polypropylene separator (19 mm in diameter). For the electrolyte solution, 0.5 M lithium bis(trifluoromethanesulfonyl)imide (LiTFSI) and 0.8 M lithium nitrate ($LiNO_3$) dissolved in dimethoxyethane (DME):1,3-dioxolane (DOL) = 1:1 (by volume) were used. To tackle issues related to the use of Li metal in high-loading Li–S batteries, relatively high contents of $LiNO_3$ were used to prepare the electrolyte solution as in our previous research.[28,29] The full-cell tests were performed by replacing the Li metal anode with the prepared graphite anode (N/P ratio = 1.2:1) and electrolyte solution with 2.5 M LiTFSI and 0.4 M $LiNO_3$ dissolved in DME:DOL = 1:1 (by volume). During the fabrication of the coin- and pouch-type cells, the ratio of the electrolyte amount to the active material content (Li_2S) was 12 μL mg^{-1}. All coin- and pouch-type cell fabrication processes were carefully performed in an Ar-filled glovebox (water and oxygen content < 0.1 ppm) to avoid contamination of Li_2S by ambient air.

Galvanostatic cycling tests were performed using a battery cycler (TOSCAT-3100; Toyo System Co.) at 30°C. For the coin-type half-cell with a Li_2S loading of 15 mg cm^{-2}, the initial cycle was performed in the voltage range of 1.9−3.6 V at 0.1 C and cycling was performed in the range of 1.8−2.8 V at 0.5 C (1 C = 1675 mA per gram of sulfur). For the coin-type full cell with a Li_2S loading of 10 mg cm^{-2}, the initial cycle was carried out in the range of 1.6−3.6 V at 0.1 C, and cycling was then conducted in the range of 1.6−2.8 V at 0.2 C. For the pouch-type half-cell with a Li_2S loading of 10 mg cm^{-2} (each side of the cathode), the initial and regular cycles were performed at 0.05 C in the ranges of 1.9−3.6 V and 1.8−2.8 V, respectively. Similarly, for the pouch-type full cells with a Li_2S loading of 10 mg cm^{-2} (each side of the cathode), the initial and regular cycles were conducted at 0.05 C in the ranges of 1.6−3.6 V and 1.6−2.8 V, respectively. The Li_2S loading of the cathode, C-rate conditions, and voltage range of the cycling test are presented in each figure. Cyclic voltammetry tests were conducted using a VMP3 (Biologic) in a voltage range of 1.9−3.6 V at 0.3 mV s^{-1}.

The electrical resistivity of the pelletized Gr/CNT and Gr electrodes with a diameter of 10 mm was analyzed using a homemade two-probe setup. The thickness of each carbon electrode was set to 0.5 mm. The ampere responses to the voltage applied to the prepared electrodes were recorded using a source meter (Keithley 2400; Keithley). Each constant voltage of 1, 2, 3, 4, and 5 mV was applied until stabilization, and then, the subsequent equilibrium current was obtained to construct an I–V plot.

2.6 | Characterization

The surface and cross-sectional morphologies of the materials were analyzed by scanning electron microscopy

(SEM) (Verios G4UC; Thermo Fisher Scientific). To observe the morphology of the materials and obtain the selected-area electron diffraction (SAED) pattern, TEM was performed using an instrument (NEO ARM; JEOL) equipped with a cooling holder (613; Gatan) and a temperature controller (1905; Gatan). During the cryo-TEM analysis, observations were conducted at 103.15 K. All samples were prepared inside an Ar-filled glovebox (water and oxygen content < 0.1 ppm) and transferred in an Ar-filled container before putting it in SEM and TEM chambers to minimize contamination. The chemical compositions of the cycled electrodes were analyzed using X-ray photoelectron spectroscopy (XPS) (K-Alpha+; Thermo Fisher Scientific). For the in situ techniques, a specialized airtight cell equipped with a window (ECC-Opto-Std, EL-CELL) was used. In situ Raman spectroscopy was performed using a radioelectric Raman system (DXR3xi; Thermo Fisher Scientific) equipped with a 532 nm laser. A high-resolution optical microscope (VHX-7000) was used to conduct in situ optical microscopy (OM). During the in situ analysis, a cell was cycled up to the voltage range of 3.6 V at 1/5 C.

3 | RESULTS AND DISCUSSION

3.1 | Preparation of the Li_2S/Gr/CNT cathode

Figure 1 shows the preparation process of the Gr/CNT composite, and the morphology and electrical properties of Gr and the Gr/CNT composite. Gr has a planar two-dimensional (2D) structure with superior electronic conductivity (10^7–10^8 S m^{-1}), and the CNTs are rolled-up Gr with a cylindrical 1D structure. The in-plane electrical conductivity of Gr (inside the layer) is high, but its through-plane conductivity is not satisfactory.[20] To reinforce the electrical property in a Gr-based Li_2S cathode, here, it was designed in such a way that the CNT forms an electrical network throughout the electrode. It is important to scatter CNTs across the Gr layer to optimally exploit the advantages of both components in the composite matrix. Figure S2 shows the aggregated Gr/CNT mixture prepared using a simple dry-mixing method. Because of the strong van der Waals interactions, Gr or CNTs easily aggregate into bundles.

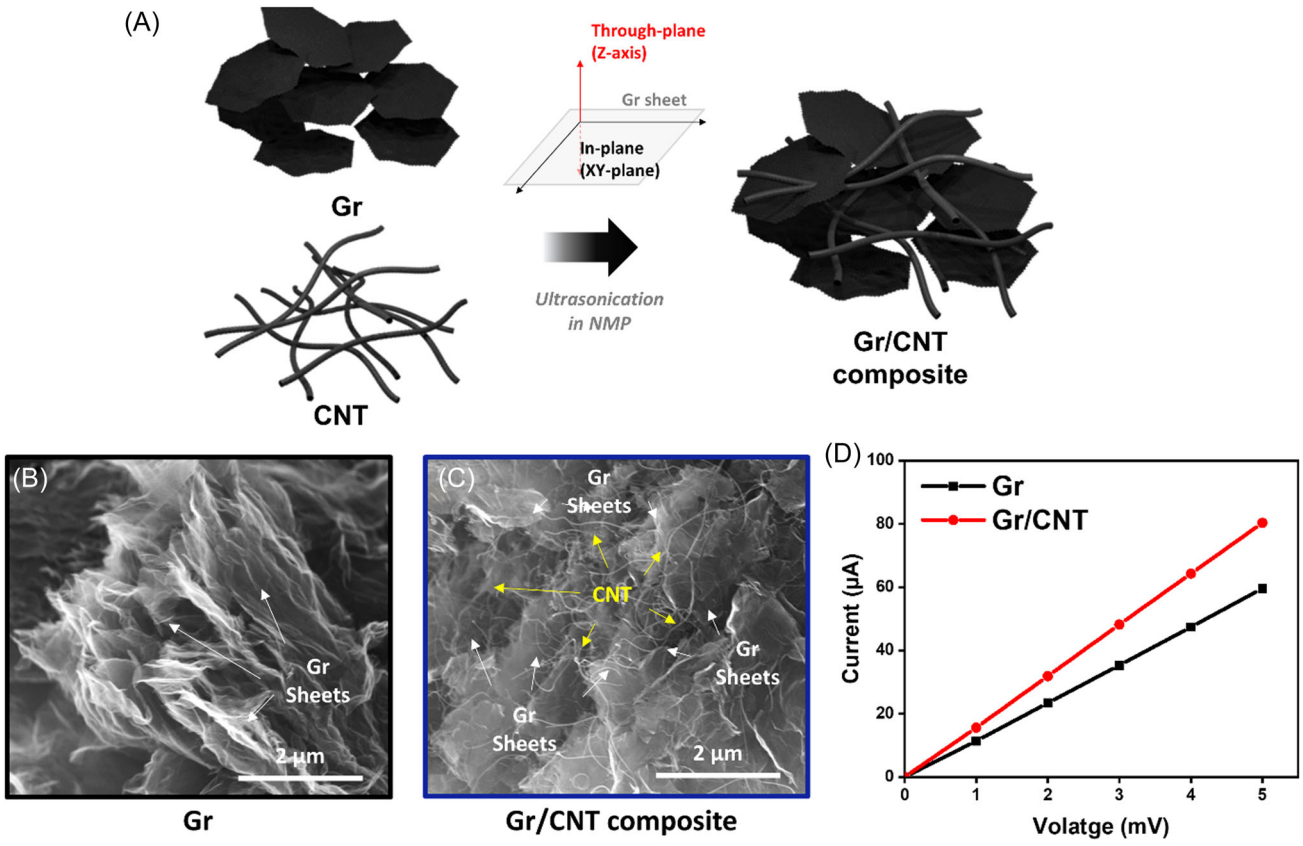

FIGURE 1 Characterization of the graphene (Gr)/carbon nanotube (CNT) (Gr/CNT) composite. (A) Schematic of the Gr/CNT composite preparation process. Scanning electron microscopy images of (B) Gr powder and (C) the Gr/CNT composite. (D) Current–voltage curves of Gr and the Gr/CNT electrode.

The proper selection of the mixing instrument and the dispersion solvent can guarantee a high degree of dispersion.[30–32] In our case, Gr and CNTs were separately ultrasonicated in NMP as the solvent without any other dispersants, and the two dispersions were then mixed together. The detailed conditions are described in the experimental section. When a Gr/CNT composite was fabricated (Figure 1B,C), a desirable 3D networking structure was observed, wherein 1D CNTs (with an average diameter of ~15 nm) interconnect each Gr particle.

To verify the effectiveness of the Gr/CNT composite compared to the Gr in terms of their electrical properties, a two-probe setup was used to observe the ampere response to the voltage applied to the prepared electrodes.[33] (Figure S3) For the analysis, carbon electrodes composed of Gr or the Gr/CNT composite were pelletized in the same manner as in the preparation of the Li_2S cathode, but without active materials (Li_2S). We assumed that electron conduction in the axial direction between the top and bottom of the high-loading Gr-based electrode could be enhanced by introducing the CNT network. Copper current collectors were placed on the top and bottom of the electrode, and the ampere response values (current) to the potential applied to the electrode (voltage) by the source meter unit were recorded. As shown in Figure 1D, ~35% higher currents were detected in the Gr/CNT electrode at each applied potential than that in the electrode with Gr alone. Gr shows the highest in-plane (single-layer) electrical conductivity among 2D materials. However, from an electrode point of view, electrical conduction is disturbed in some nano/micro-scale regions owing to the relatively low electrical conductivity of through-plane and over-the-Gr particles. On the other hand, CNTs form a network in all directions in the electrode, so they act as electrical highways from one point to another and confer uniform conductivity to the entire electrode. This analysis was the first step in analyzing the role of the CNT in the electrode from the fabricated Gr/CNT composite matrix.

Next, to fabricate the compact Li_2S/Gr/CNT cathode, a mixture composed of commercial microscale Li_2S and our Gr/CNT composite was prepared using a mechanical ball-milling process. Then, the Li_2S/Gr/CNT composite powder was pelletized in a mold under a high pressure of 1 GPa (Figure 2A).

Figure 2B,C shows cross-sectional SEM images of the compact Li_2S/Gr/CNT cathode with a Li_2S loading of 15 mg cm^{-2}. The measured thickness of the compact cathode with a high Li_2S loading was 166 μm.

As shown in Figure 2C, the dispersed Li_2S particles with sizes of 1–5 μm were surrounded by the Gr/CNT composite matrix, and CNTs connected each Gr particle, forming a 3D network structure. The corresponding TEM image confirms the structural characteristics of the Li_2S/Gr/CNT cathode. The bright-field TEM images in Figure 2D,F demonstrate that the Li_2S particles were completely encapsulated by 2D Gr sheets with an entangled network of 1D CNTs embedded within these sheets. The CNT network provided robust electrical

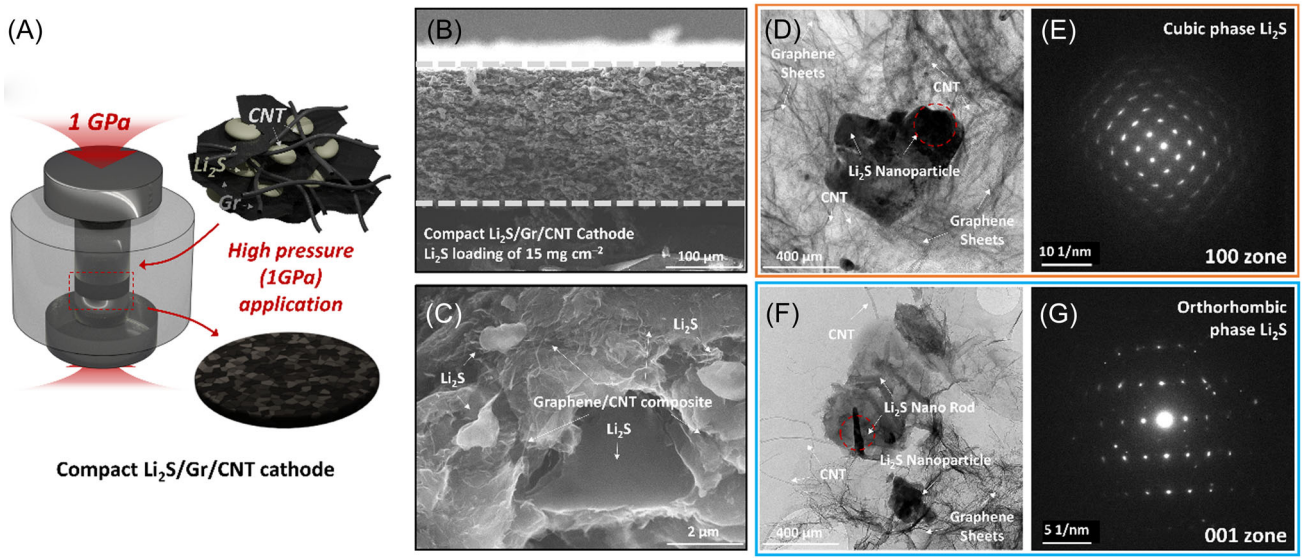

FIGURE 2 Characterization of the compact Li_2S/Gr/CNT cathode. (A) Schematic of the fabrication and structure of a compact Li_2S/Gr/CNT cathode. (B,C) Cross-sectional SEM images, (D,F) bright-field TEM images of a compact Li_2S/Gr/CNT cathode, and (E,G) the corresponding selected-area electron diffraction patterns of the polymorph marked in panels (D,F). CNT, carbon nanotube; Gr, graphene; Li_2S, lithium sulfide; SEM, scanning electron microscopy; TEM, transmission electron microscopy.

pathways that connected the active materials throughout the electrode. The [100] zone SAED pattern of the Li_2S particle confirms the face-centered cubic structure of Li_2S (Figure 2E). In addition to the cubic-phase Li_2S, the TEM image in Figure 2F shows the presence of flattened and rod-shaped Li_2S nanoparticles, whose SAED pattern was indexed as the [001] zone of the orthorhombic Li_2S phase (Figure 2G). At a pressure above 12 GPa, the *Fm3m* antifluorite structure of Li_2S transforms into an orthorhombic *Pnma* phase. Upon removal of high pressure, this high-pressure orthorhombic phase reverts to the cubic phase.[34]

It is conjectured that here, the cubic Li_2S phase partially transformed into the high-pressure form of orthorhombic phase during the pelletization of the Li_2S/Gr/CNT composite powder. A highly localized compressive stress during deformation may have developed and exceeded the critical stress required for the transformation, with the Gr sheets confining Li_2S and restraining its lateral expansion.[28,34] Thus, the TEM analysis revealed that the Li_2S particles, which were tightly encapsulated by the Gr sheets and entangled by the CNTs, existed in multiple phases. Additional examples of the presence of metastable orthorhombic Li_2S are shown in Figure 3, which summarizes the main microstructural features of the compact Li_2S cathode fabricated by pelletization under high pressure. A similar observation was also made in the previous report.[28]

3.2 | Electrochemical performance

Figure 4 shows the electrochemical performance of the compact Li_2S/Gr/CNT cathode. For comparison, the Li_2S/Gr and Li_2S/CNT cathodes fabricated in the same manner were also tested (explained in the Section 2.2). Figure 4A shows the first voltage profile cycled at 0.1 C of each cathode with an ultrahigh Li_2S loading of 15 mg cm^{-2} and a Li anode.

The compact Li_2S/Gr/CNT cathode delivered a higher first charging capacity for Li_2S activation than the Li_2S/Gr and Li_2S/CNT cathodes. This result suggests the effect of adding CNTs on the Gr-based Li_2S cathode. The content of active sulfur in the cathode and the delivered capacity of the Li–S battery have a trade-off relationship. In this case, when Li_2S accounted for 75% of the total content and carbon content was as low as 25%, the role of Gr and the CNTs as conductive carbon materials became obvious. The 2D planar morphology of Gr provided a large contact area with the bulk Li_2S, thus playing an important role in the exchange of electrons with insulating active materials, Li_2S, although the 1D CNTs (<20 nm in diameter) do not function well in activating micro-sized bulk Li_2S. As illustrated in Figure 4C, meanwhile, only a small amount of CNTs (Gr:CNT = 7:1 by weight and 3.125% of the total weight of the cathode) in place of the Gr finely enhanced the activation of the Li_2S, forming a 3D network and eliminating

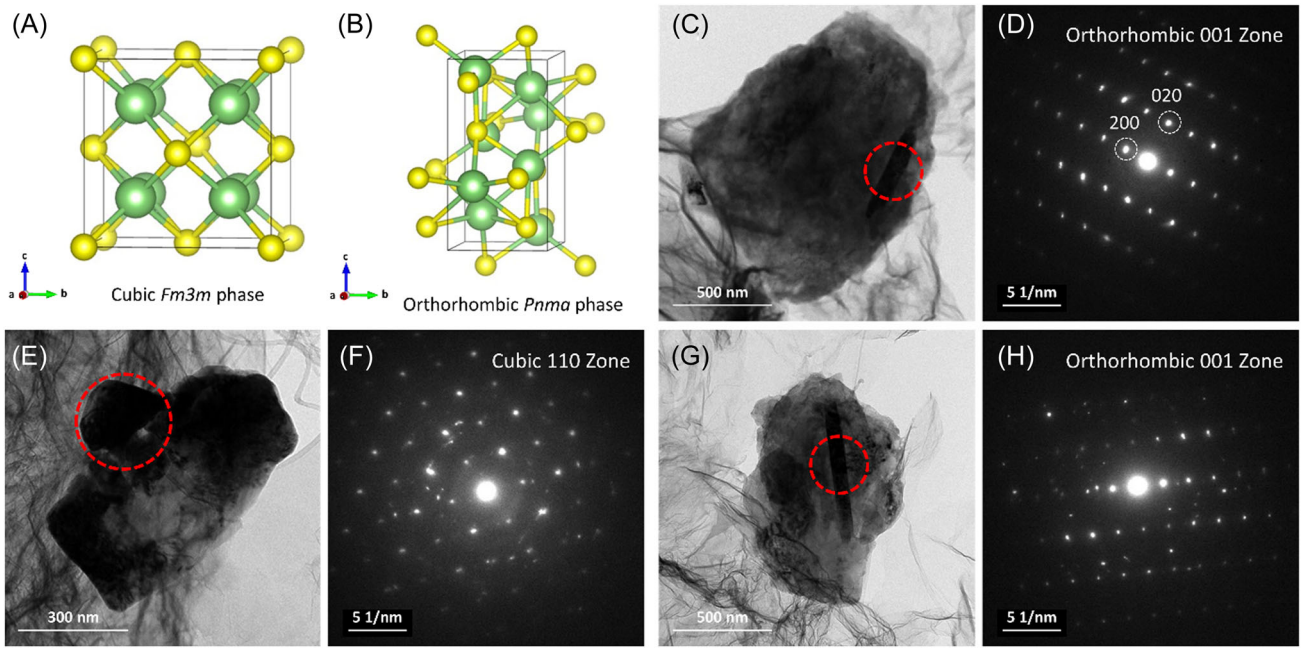

FIGURE 3 Characterization of the Li_2S polymorph in the compact Li_2S/Gr/CNT cathode. Schematics of the unit cell structure of Li_2S: (A) cubic *Fm3m* phase and (B) orthorhombic *Pnma* phase. (C,E,G) Bright-field TEM images of the Li_2S polymorph in the compact Li_2S/Gr/CNT cathode and (D,F,H) the corresponding SAED patterns of the polymorph marked in panels (C,E,G). CNT, carbon nanotube; Gr, graphene; Li_2S, lithium sulfide; SAED, selected-area electron diffraction.

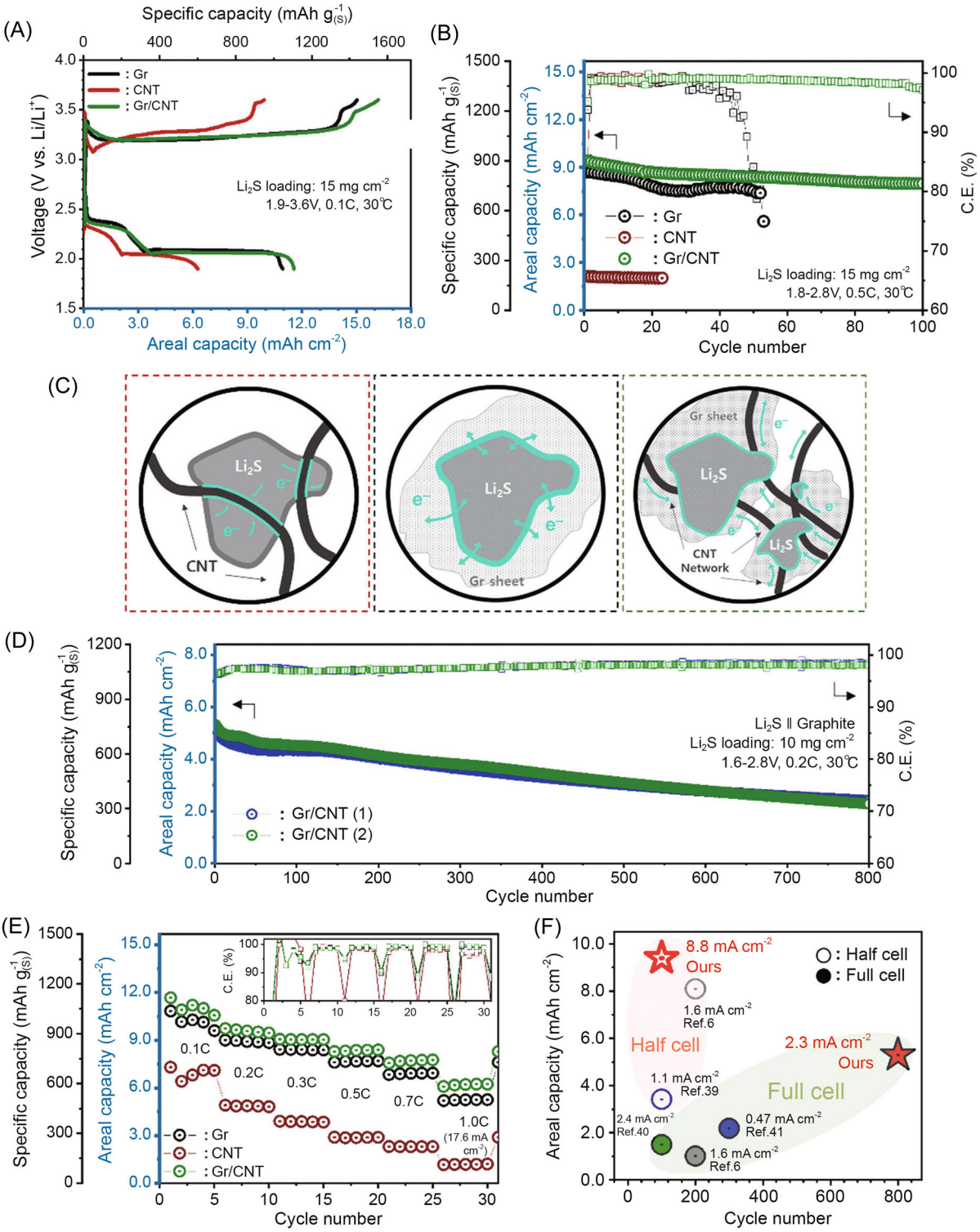

FIGURE 4 Electrochemical performance of the compact Li_2S/Gr/CNT cathode in a Li–S cell. (A) Initial cycle voltage profiles of Li–S half-cells using a compact Li_2S/Gr/CNT, Li_2S/Gr, or Li_2S/CNT cathode with a Li_2S loading of 15 mg cm^{-2} at 0.1 C in the voltage range of 1.9–3.6 V and (B) subsequent cycling performed at 0.5 C in the voltage range of 1.8–2.8 V. (C) Illustration showing the interplay between the bulk Li_2S particle and the two different carbon materials. (D) Cycling test of Li–S full cells using the compact Li_2S/Gr/CNT cathode with a Li_2S loading of 10 mg cm^{-2} at 0.2 C in the voltage range of 1.6–2.8 V. The full cells were fabricated using the high-loading graphite anode (N/P ratio: 1.2). (E) Rate capability of Li–S half-cells using a compact Li_2S/Gr/CNT with a Li_2S loading of 15 mg cm^{-2}; current rates from 0.1 to 1.0 C (17.6 mA cm^{-2}). All tests were performed at 30°C. (F) Comparison of the cycling performance of previously reported Li_2S-based Li–S cells. CNT, carbon nanotube; Gr, graphene; Li_2S, lithium sulfide.

electrically isolated parts throughout the whole cathode (Figure 4A). However, as CNT content was increased more than 3.125%, the Li_2S activation was lowered. (Figure S4) Note that the voltage profile of the first charging process of the compact Li_2S/Gr/CNT cathode did not follow the general charging curve of the Li_2S-based Li–S battery. According to previously reported results,[7,21,35] the activation of Li_2S in the early stage of the first charge requires a high voltage owing to the difficulty of lithium diffusion from the insulating Li_2S. Meanwhile, LiPs is formed, and the charging voltage decreases owing to the function of LiPs as a redox mediator, which facilitates the oxidation process. However, the initial charging voltage of the compact Li_2S/Gr/CNT cathode started above 3.2 V versus Li/Li^+ and was maintained throughout the charging process, with a gradually increasing trend. This voltage profile indicates the direct conversion process in which Li_2S is directly converted into S_8 without forming LiPs.[26–28] This unique conversion process is thoroughly identified in the next section using in situ spectral and optical techniques. The cyclic voltammogram in Figure S5 showed good agreement with the first cycle voltage profile of each cathode (Figure 4A), showing better electro-chemical activities in the compact Li_2S/Gr/CNT cathode than in the other two cathodes. In Figure 4B, the cycling performance at 0.5 C of the Li–S cell using each cathode is compared. As expected from the first charging/discharging capacity, the compact Li_2S/Gr/CNT cathode showed a higher discharge capacity of 899.6 mAh g^{-1} (11.5 mAh cm^{-2}) than the Li_2S/Gr cathode (833.4 mAh g^{-1}) and the Li_2S/CNT (205.6 mAh g^{-1}) cathode. Furthermore, the compact Li_2S/Gr/CNT cathode showed stable cycling with a high Coulombic efficiency over 100 cycles. By contrast, the Li_2S/Gr cathode showed a steep capacity drop, with Coulombic efficiency fading after approximately 50 cycles.

To investigate the role of CNTs in improving cycling performance, a Li_2S/Gr cathode after cell failure and a reproduced compact Li_2S/Gr/CNT cathode cycled the same number of times were retrieved. The SEM image of the cycled Li_2S/Gr cathode in Figure 5A shows the severe surface passivation on the Gr particles, which may hinder electrical conduction over the particles throughout the electrode. XPS analysis revealed that sulfate, polythionate, and thiosulfate species, in addition to the remaining polysulfide-related species, predominantly existed on the cathode surface (Figure 5C)[19,29,36,37]. On the other hand, in the cycled Li_2S/Gr/CNT cathode (Figure 5B), less surface passivation was apparent on the Gr particles, and the XPS results also demonstrated fewer sulfate and polythionate species (Figure 5D). Notably, morphologically intact CNTs dispersed throughout the electrode maintained good electrical connections. Except for a small portion, the majority of the CNT surfaces were not densely covered by precipitates, thus maintaining the original morphology. From these observations, we can infer that Gr, which has a large contact area with active materials, plays a major role in driving the electrochemical conversion process of sulfur species, whereas CNTs maintain uniform and high electrical conduction throughout the electrode, helping the conversion reaction proceed effectively and sustainably.

The key advantage of Li_2S-based Li–S batteries is that they can use Li-metal-free anodes because Li_2S can provide the Li required for cell operation in the absence of Li metal as a Li source. To assess the feasibility of the compact Li_2S/Gr/CNT cathode as a potential cathode for practical applications, Li–S full batteries using natural graphite as an alternative anode were fabricated. Natural graphite is a commercially available anode material with good cycling stability. For the electrolyte solution, a Li-ion coordination structure-tailored ethereal electrolyte, which is known to be compatible with graphite anodes, was used.[38] As shown in Figure 4D, the compact Li_2S/Gr/CNT cathode applied in the Li–S full batteries delivered an areal capacity of 5.3 mAh cm^{-2} at 0.2 C and operated for more than 800 cycles, even at a high Li_2S loading of 10 mg cm^{-2}.

To the best of our knowledge, this is the first report demonstrating Li–S full batteries loaded with such a high level of Li_2S and the unprecedented cycling stability of such high-loading Li–S batteries. This notable electrochemical half-/full-cell performance is due to (1) the compact geometry of the cathode enabling close contact between Gr and the active materials for efficient electron exchange, (2) the role of CNTs, which form an electrical network through the electrode, thus inducing and maintaining uniform reactions in the entire electrode, and (3) the use of a Li-metal-free anode with good cycling stability in the case of a full cell, avoiding the safety hazard of Li metal anodes. In addition, the compact Li_2S/Gr/CNT cathode showed high rate capability even at a current density of 17.6 mA cm^{-2}, delivering an areal capacity higher than 6 mAh cm^{-2} (Figure 4E). The cycling performance of the compact Li_2S/Gr/CNT cathode with a high Li_2S loading is compared with that of cathodes reported in the literature thus far in Figure 4F[6,39–41] and Table S1.

3.3 | Direct conversion reaction during first charge

To investigate the distinct first charging process of the compact Li_2S/Gr/CNT cathode, in situ Raman

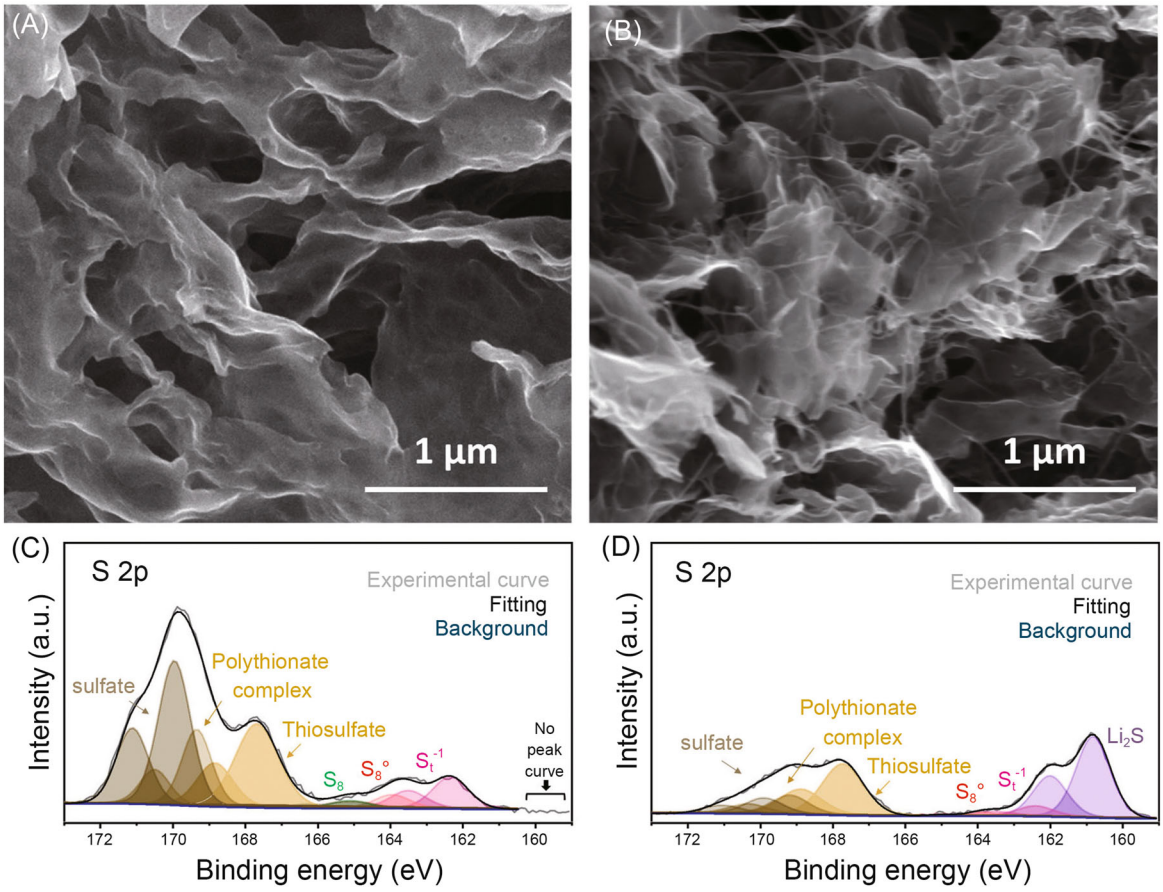

FIGURE 5 Characterization of the cycled cathode. SEM images of the cycled (A) Li_2S/Gr cathode after cell failure and (B) compact Li_2S/Gr/CNT cathode cycled the same number of times as the cell in panel (A). XPS S 2p spectra of the cycled (C) Li_2S/Gr and (D) Li_2S/Gr/CNT cathodes. CNT, carbon nanotube; Gr, graphene; Li_2S, lithium sulfide; SEM, scanning electron microscopy; XPS, X-ray photoelectron spectroscopy.

spectroscopy, in situ OM, and cryo-TEM analysis were conducted. To monitor the changes occurring at the Li_2S cathode in real time, a test cell equipped with a quartz window on the cathode side was adopted. As a test cell was electrochemically charged by connecting it to the galvanostat, Raman spectroscopy and high-resolution digital OM were performed. The setup for the in situ analysis is presented in Figure 6A. Figure 6B shows the obtained Raman spectra during the charging process as a contour plot. At the beginning of the charge, the spectrum of the compact Li_2S/Gr/CNT cathode showed a Li_2S band at 373 cm^{-1},[42–44] but the intensity of the Li_2S band gradually weakened as charging proceeded.

Interestingly, the intensities of the characteristic peaks of S_8 at 152, 220, and 473 cm^{-1}[42,43] appear early from a 12% state of charge (SoC). In addition, high and low polysulfide bands, which primarily appear at 398 cm^{-1} (S–S stretching mode in S_8^{n-}, $n = 1$, 2) and 453 cm^{-1} (stretching mode of S_4^{2-}), respectively, were not observed before the formation of the S_8.[42,45,46] During the well-known charging process of Li–S batteries, Li_2S is converted into LiPs, which is then finally converted into S_8 at the end of the charge.[7,21,35,47,48] The early detection of S_8 and the absence of polysulfide bands during the entire charging process provide strong evidence for the direct conversion of the Li_2S into S_8 without the formation of polysulfide intermediates. The compact Li_2S/Gr/CNT cathode was charged to 50% of the full charge, and the cathode was then retrieved and analyzed by cryo-TEM (Figure 7). The bright-field TEM image shows agglomerates of nanoparticles with sizes less than 10 nm interspersed with relatively larger particles (10–100 nm) embedded in the Gr/CNT composite (Figure 7A,C,E).

No elongated orthorhombic Li_2S, which is a metastable phase at atmospheric pressure, was detected, suggesting that the metastable Li_2S was readily delithiated, thus promoting the conversion of Li_2S. For comparison, bright-field TEM images of a Li_2S/Gr cathode at a 50% SoC are shown in Figure S6. Similarly, agglomerates of Li_2S nanoparticles within Gr sheets were observed, and the

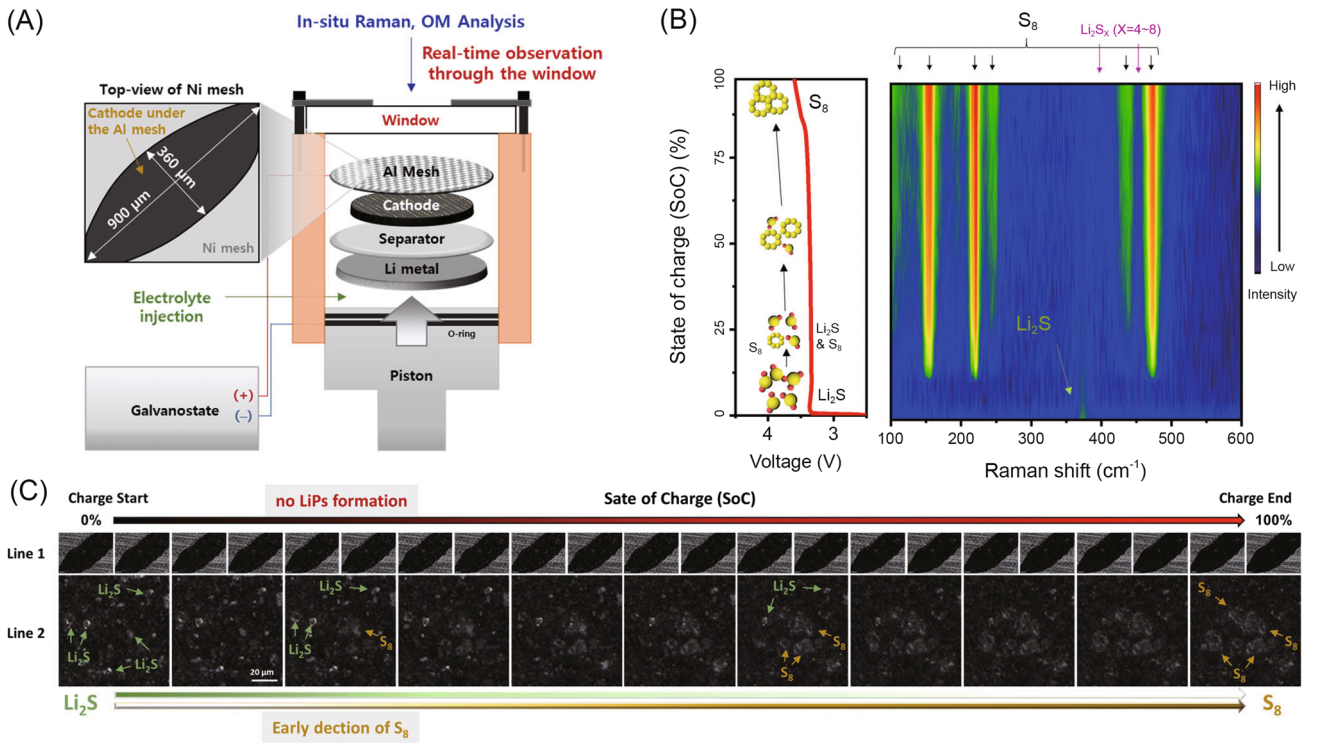

FIGURE 6 Unique activation process of Li_2S in the compact Li_2S/Gr/CNT cathode during the first charge. (A) Schematic of the setup for the in situ Raman analysis and in situ optical microscopy (OM) analysis. (B) First charge voltage profile and contour plot of the in situ Raman analysis during the first charge process. (C) Snapshots from the in situ OM analysis during the first charge process. In panel (C), line 1 shows the Al mesh and cathode viewed through a hole in the Al mesh (refer to the schematic, shown in (A)), and line 2 shows high-magnification images of the cathode. CNT, carbon nanotube; Gr, graphene; Li_2S, lithium sulfide.

elongated orthorhombic Li_2S phase was not observed. However, different from the Li_2S/Gr/CNT cathode, relatively large Li_2S particles (the cubic phase shown in Figure S6D) with sizes ranging from 200 to 500 nm were detected in the Li_2S/Gr cathode. These large Li_2S particles in the Li_2S/Gr cathode substantiate the efficacy of the CNT networks in inducing uniform reactions across the entire electrode. For the Li_2S/Gr/CNT cathode, accompanying SAED patterns confirm the presence of the cubic Li_2S phase and show an additional ring pattern with a d-spacing of 4.5 Å, distinct from the ring patterns of the Gr/CNT composite (Figure 7B,D, and Figure S7). This additional pattern could be matched to β-S_8 (PDF#: 65-6467), delithiated from the Li_2S during the conversion process. In contrast to the general "solid–liquid–solid" mechanism, in which S_8 appears at the end of the charging process,[42,43] the TEM analysis results indicate that S_8 and Li_2S coexist even at 50% SoC, resulting from the direct conversion ($Li_2S \rightarrow S_8$) reaction mechanism. β-S_8, which is vulnerable to damage by an electron beam, was observed using cryo-TEM at a low temperature (103.15 K); to the best of our knowledge, this is the first simultaneous observation of Li_2S and S_8 in the direct conversion process.

Next, using high-resolution OM, we observed the conversion process of Li_2S in a compact Li_2S/Gr/CNT cathode in real time. The surface of the cathode beneath the Al mesh was analyzed through a mesh hole (width: 360 μm. Height: 900 μm) under the window. The optical images in line 1 of Figure 6C show the Al mesh and the cathode viewed through the mesh hole, and line 2 shows magnified optical images of the cathode during the overall first charging process. The low-magnification images in line 1 visually confirmed that yellow liquid LiPs was not induced during the entire charging process. For comparison, an optical image showing an environment in which yellowish LiPs are present is shown in Figure S8. In the high-magnification images in line 2, the conversion process of the Li_2S into S_8 can be visualized. Initially, the Li_2S particles gradually disappeared, and new S species emerged in the immediate vicinity. In this case, new S species considered to be β-S_8 also appeared first at an SoC of ~10% and then gradually continued to emerge. At the end of the charging process, the Li_2S particles that existed in the early stages of charging finally disappeared, and only S_8 was apparent. The bright-field TEM images of the Li_2S/Gr/CNT cathode

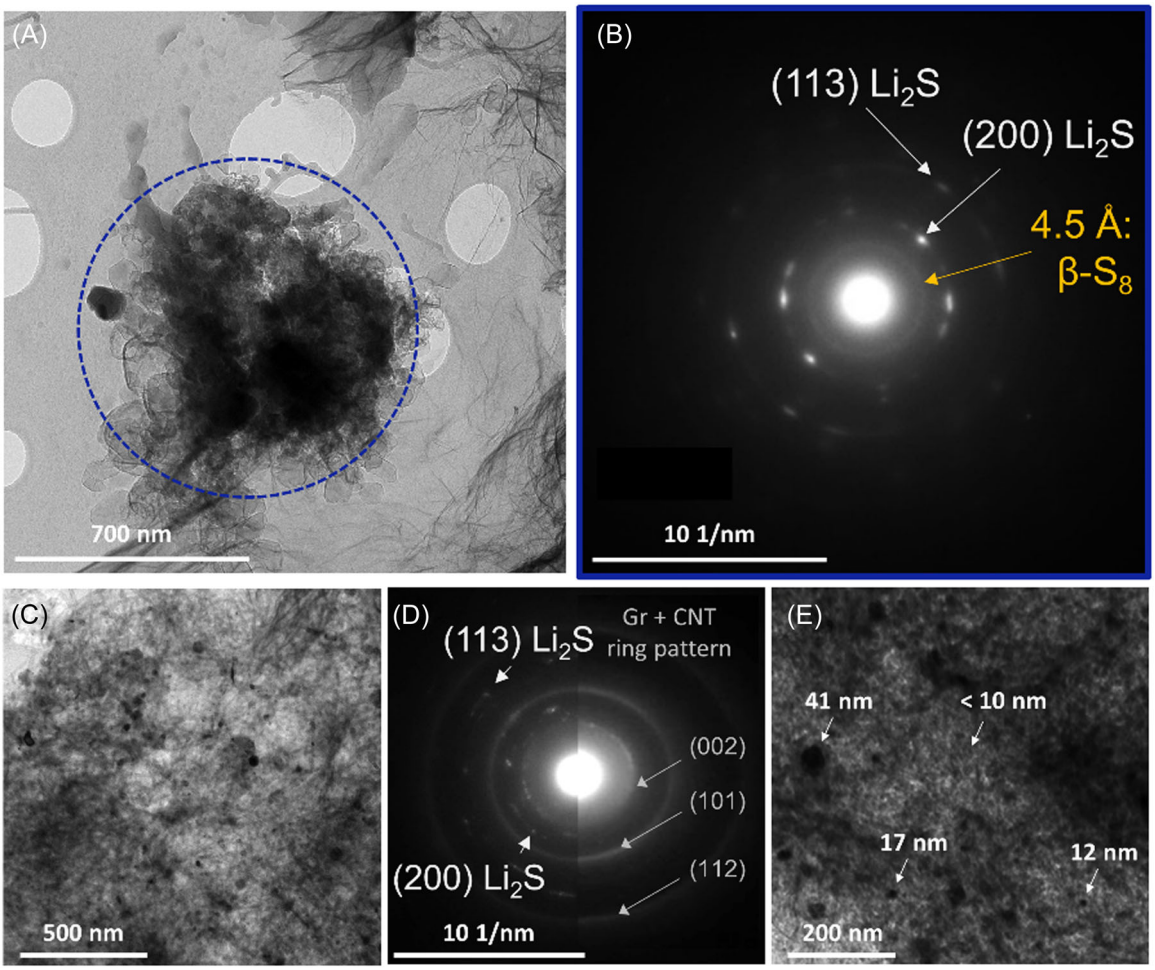

FIGURE 7 Characterization of the compact Li_2S/Gr/CNT cathode in the 50% state of charge (SoC) during the first charge. (A,C,E) Bright-field TEM images of the Li_2S/S_8 polymorph in the compact Li_2S/Gr/CNT cathode. (B,D) Corresponding SAED patterns from panels (A,C). CNT, carbon nanotube; Gr, graphene; Li_2S, lithium sulfide; SAED, selected-area electron diffraction; TEM, transmission electron microscopy.

at 100% SoC show that Li_2S nanoparticles nearly disappeared at the end of charging, and sulfur compounds, whose morphology was difficult to specify, were observed throughout the Gr/CNT composite (Figure S9). The in situ OM observations correspond well with the in situ Raman and cryo-TEM analyses. In summary, a series of analyses provided consistent evidence of a direct conversion reaction (from Li_2S to S_8) occurring during the first charging process of a compact Li_2S/Gr/CNT cathode.

3.4 | Scaled-up pouch-type cell using the Li_2S/Gr/CNT cathode

The fabrication of pouch-type cells with practical utility is important for evaluating the feasibility of the proposed concept; however, because of technical difficulties, including issues related to handling of Li_2S, Li_2S-based Li–S batteries are rarely constructed using pouch-type batteries. To the best of our knowledge, this is the first study to fabricate Li_2S-based multistacked pouch-type half and full batteries using a compact Li_2S/Gr/CNT cathode with such a high Li_2S loading (10 mg cm^{-2} on each side of the cathode; Figure 8). Their configurations are shown in Figure 8A. The pouch-type half and full batteries deliver 6.7 and 5.3 mAh cm^{-2}, respectively, at 0.05 C, and show capacity retentions of 86.4% and 92.5% after 50 cycles, respectively (Figure 8B,C). The energy density of the large-sized cathode used in the pouch-type cell was 1006.3 Wh kg^{-1}, which presented a superior energy density of the proposed Li_2S/Gr/CNT cathode (calculation details are presented in Table S2).

Interestingly, the half battery showed a fluctuating Coulombic efficiency and capacity after 30 cycles, whereas the pouch-type full battery (free of Li metal)

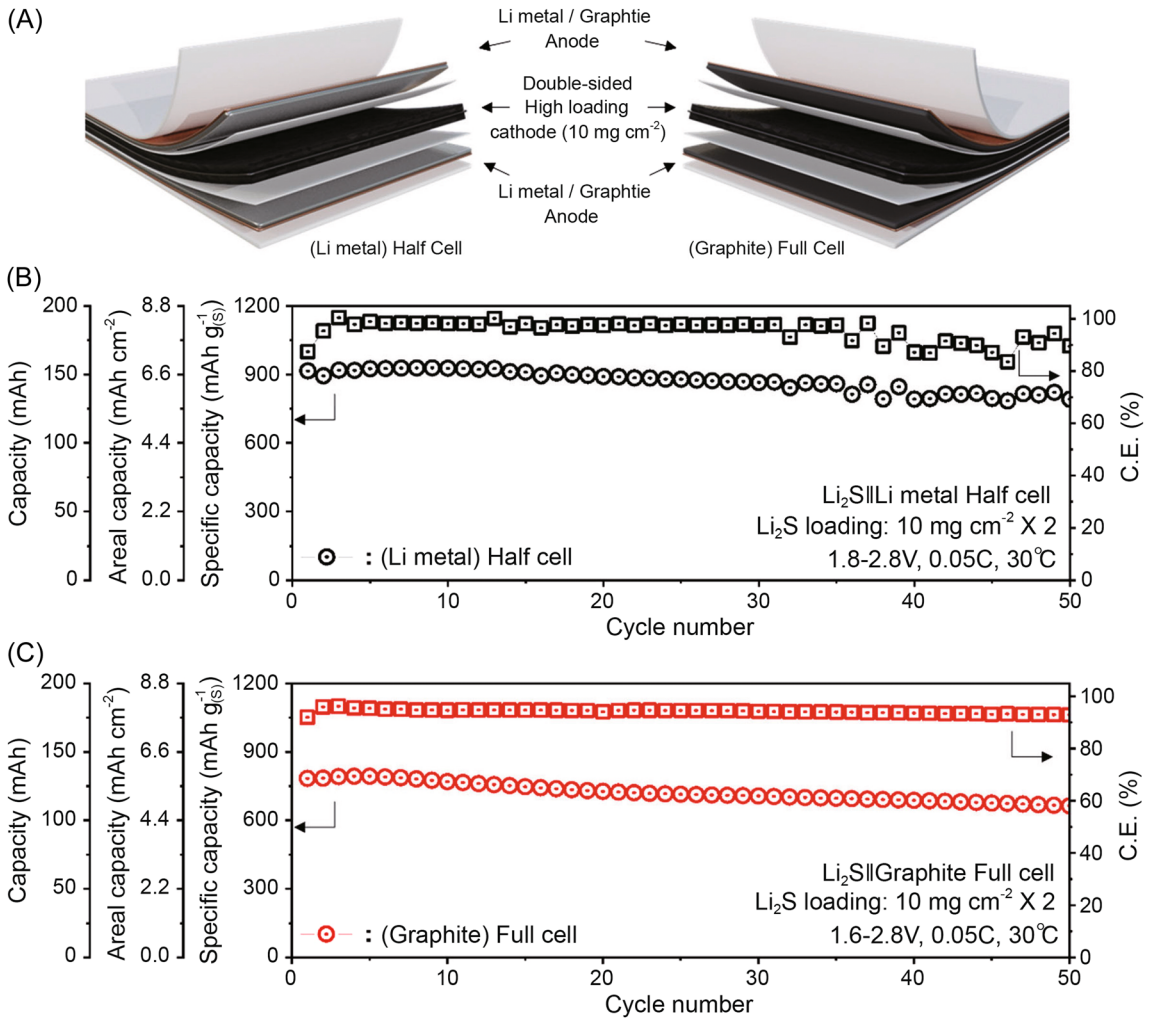

FIGURE 8 Pouch-type half and full Li–S cells fabricated using the compact Li_2S/Gr/CNT cathode. (A) Schematic of the pouch-type half and full cells. For the cathode, double-sided compact Li_2S/Gr/CNT cathodes with a Li_2S loading of 10 mg cm^{-2} (on each side of the cathode) were used. The full cell was fabricated using the high-loading graphite anode (N/P ratio: 1.2). (B) The half-cell was operated in the range of 1.8–2.8 V and (C) the full cell was operated in the range of 1.6–2.8 V. All tests were performed at 0.05 C and 30°C. CNT, carbon nanotube; Gr, graphene; Li_2S, lithium sulfide.

demonstrated stable cycling for the full 50 cycles. As shown in the digital photograph of the Li metal anode from the pouch-type half-battery after 50 cycles (Figure S10), Li metal was found to be unevenly depleted, especially at the center of the electrode, and the copper current collector was exposed. This shows the instability of Li metal anodes in Li–S batteries, in which uncontrollable LiPs dissolved into the electrolyte, inducing shuttle reactions and forming a thick passivation layer on the Li metal, thereby causing uneven electrochemical reactions on both electrodes. These results highlight the need to develop a highly stable Li-metal-free anode and a Li_2S-based Li–S battery that can utilize this anode.

4 | CONCLUSION

In this study, we focused on the fabrication of a high-performance Li_2S-based cathode; thus, we proposed a rationally designed compact Li_2S/Gr/CNT cathode using a high-pressure pelletization method. The planar morphology of Gr allowed large-area contact with bulk Li_2S, thus inducing the facile activation of Li_2S, and the electrical network formed by the CNTs maintained a uniform, facile reaction during prolonged cycling. In addition, the compact geometry of the cathode enables close contact between the carbon matrix and the active materials. Compared to previously reported results on Li_2S-based Li–S batteries, the half and full Li–S batteries using a compact Li_2S/Gr/CNT

cathode showed unprecedented high areal capacity and cycle life, as shown in Figure 4F and Table S1. Notably, a direct conversion reaction (from Li_2S to S_8) during the first charge was observed in the compact Li_2S/Gr/CNT cathode and it was investigated using in situ techniques and cryo-TEM. In the proposed compact Li_2S/Gr/CNT cathode, the highly conductive carbon matrix, the compact geometry of the electrode, the highly deformed metastable Li_2S (formed during the high-pressure pelletization), and this unique direct conversion reaction all contributed to the effective activation of Li_2S. Even with lean electrolyte conditions (electrolyte amount to Li_2S weight ratio of 7 $\mu L\,mg^{-1}$), notably, the cathode shows high electrochemical activity with a practical areal capacity of ~9.7 $mAh\,cm^{-2}$ at 0.2 C (Figure S11). Finally, large-size pouch-type Li_2S-based half and full Li–S batteries with a high Li_2S loading of 10 $mg\,cm^{-2}$ were also demonstrated, providing insights into the importance of anode selection in Li–S batteries. It is believed that the advantages of Li_2S-based Li–S batteries, which can avoid issues related to safety hazards of Li metal anodes, will effectively accelerate the practical use of Li–S batteries. We hope that our well-established understanding of carbon materials, this newly proposed cathode, and the electrochemical performance observed in this study will provide useful guidelines for further development of Li–S batteries.

ACKNOWLEDGMENTS

This work was supported by the Samsung Research Funding & Incubation Center of Samsung Electronics under Project Number SRFC-MA1901-06 and a Human Resources Development Program (No. 20214000000320) as part of a Korea Institute of Energy Technology Evaluation and Planning (KETEP) grant, funded by the Ministry of Trade, Industry, and Energy of the Korean government.

CONFLICTS OF INTEREST

The authors declare no conflicts of interest.

ORCID

Yang-Kook Sun http://orcid.org/0000-0002-0117-0170

REFERENCES

1. Pang Q, Liang X, Kwok CY, Nazar LF. Advances in lithium–sulfur batteries based on multifunctional cathodes and electrolytes. *Nat Energy*. 2016;1(9):16132.
2. Peng H-J, Huang J-Q, Cheng X-B, Zhang Q. Review on high-loading and high-energy lithium-sulfur batteries. *Adv Energy Mater*. 2017;7(24):1700260.
3. Ji X, Lee KT, Nazar LF. A highly ordered nanostructured carbon–sulphur cathode for lithium–sulphur batteries. *Nat Mater*. 2009;8(6):500-506.
4. Hagen M, Hanselmann D, Ahlbrecht K, Maça R, Gerber D, Tübke J. Lithium-sulfur cells: the gap between the state-of-the-art and the requirements for high energy battery cells. *Adv Energy Mater*. 2015;5(16):1401986.
5. Shin W, Lu J, Ji X. ZnS coating of cathode facilitates lean-electrolyte Li-S batteries. *Carbon Energy*. 2019;1(2):165-172.
6. Tan G, Xu R, Xing Z, et al. Burning lithium in CS_2 for high-performing compact Li_2S–graphene nanocapsules for Li–S batteries. *Nat Energy*. 2017;2(7):17090.
7. Ye H, Li M, Liu T, Li Y, Lu J. Activating Li_2S as the lithium-containing cathode in lithium–sulfur batteries. *ACS Energy Lett*. 2020;5(7):2234-2245.
8. Kong L, Wang L, Ni Z, Liu S, Li G, Gao X. Lithium–magnesium alloy as a stable anode for lithium–sulfur battery. *Adv Funct Mater*. 2019;29(13):1808756.
9. Bieker G, Küpers V, Kolek M, Winter M. Intrinsic differences and realistic perspectives of lithium-sulfur and magnesium-sulfur batteries. *Commun Mater*. 2021;2(1):37.
10. Nanda S, Manthiram A. Lithium degradation in lithium–sulfur batteries: insights into inventory depletion and interphasial evolution with cycling. *Energy Environ Sci*. 2020;13(8):2501-2514.
11. Yang K, Yang L, Wang Z, et al. Constructing a highly efficient aligned conductive network to facilitate depolarized high-areal-capacity electrodes in Li-ion batteries. *Adv Energy Mater*. 2021;11(22):2100601.
12. de la Torre-Gamarra C, Sotomayor ME, Sanchez J-Y, et al. High mass loading additive-free $LiFePO_4$ cathodes with 500 μm thickness for high areal capacity Li-ion batteries. *J Power Sources*. 2020;458:228033.
13. Zhou G, Paek E, Hwang GS, Manthiram A. Long-life Li/polysulphide batteries with high sulphur loading enabled by lightweight three-dimensional nitrogen/sulphur-codoped graphene sponge. *Nat Commun*. 2015;6:7760.
14. Fang R, Zhao S, Pei S, et al. Toward more reliable lithium–sulfur batteries: an all-graphene cathode structure. *ACS Nano*. 2016;10(9):8676-8682.
15. Hwang J-Y, Kim HM, Lee S-K, et al. High-energy, high-rate, lithium-sulfur batteries: synergetic effect of hollow TiO_2-webbed carbon nanotubes and a dual functional carbon-paper interlayer. *Adv Energy Mater*. 2016;6(1):1501480.
16. Kang H-S, Park E, Hwang J-Y, et al. A scaled-up lithium (ion)-sulfur battery: newly faced problems and solutions. *Adv. Mater. Technol*. 2016;1(6):1600052.
17. Cao J, Zhu B, Zheng K, et al. Carbon nanotube-based materials for lithium–sulfur batteries. *J Mater Chem A*. 2019;7(29):17204-17241.
18. Gai L, Zhao C, Zhang Y, Hu Z, Shen Q. Constructing a multifunctional mesoporous composite of metallic cobalt nanoparticles and nitrogen-doped reduced graphene oxides for high-performance lithium-sulfur batteries. *Carbon Energy*. 2022;4(2):142-154.
19. Kim H, Bang S, Min K-J, Ham Y-G, Park S-J, Sun Y-K. Achieving high-performance Li–S batteries via polysulfide adjoining interface engineering. *ACS Appl Mater Interfaces*. 2021;13(33):39435-39445.
20. Kinloch IA, Suhr J, Lou J, Young RJ, Ajayan PM. Composites with carbon nanotubes and graphene: an outlook. *Science*. 2018;362(6414):547-553.
21. Yang Y, Zheng G, Misra S, Nelson J, Toney MF, Cui Y. High-capacity micrometer-sized Li_2S particles as cathode materials

for advanced rechargeable lithium-ion batteries. *J Am Chem Soc*. 2012;134(37):15387-15394.
22. Li S, Leng D, Li W, et al. Recent progress in developing Li_2S cathodes for Li–S batteries. *Energy Storage Mater*. 2020;27:279-296.
23. Yuan H, Chen X, Zhou G, et al. Efficient activation of Li_2S by transition metal phosphides nanoparticles for highly stable lithium–sulfur batteries. *ACS Energy Lett*. 2017;2(7):1711-1719.
24. Shi P, Liang X, Xu K, et al. Sulfone-assisted-NH_4I as electrolyte additive with synergistic dissolution and catalysis effects on reducing the activation voltage of Li_2S cathode. *Chem Eng J*. 2020;398:125608.
25. Zu C, Klein M, Manthiram A. Activated Li_2S as a high-performance cathode for rechargeable lithium–sulfur batteries. *J Phys Chem Lett*. 2014;5(22):3986-3991.
26. Vizintin A, Chabanne L, Tchernychova E, et al. The mechanism of Li_2S activation in lithium-sulfur batteries: can we avoid the polysulfide formation? *J Power Sources*. 2017;344:208-217.
27. Zhang L, Sun D, Feng J, Cairns EJ, Guo J. Revealing the electrochemical charging mechanism of nanosized Li_2S by in situ and operando X-ray absorption spectroscopy. *Nano Lett*. 2017;17(8):5084-5091.
28. Hwang J-Y, Shin S, Yoon CS, Sun Y-K. Nano-compacted Li_2S/graphene composite cathode for high-energy lithium–sulfur batteries. *ACS Energy Lett*. 2019;4(12):2787-2795.
29. Kim HM, Hwang J-Y, Bang S, et al. Tungsten oxide/zirconia as a functional polysulfide mediator for high-performance lithium–sulfur batteries. *ACS Energy Lett*. 2020;5(10):3168-3175.
30. Green MJ. Analysis and measurement of carbon nanotube dispersions: nanodispersion versus macrodispersion. *Polym Int*. 2010;59(10):1319-1322.
31. Huang YY, Terentjev EM. Dispersion of carbon nanotubes: mixing, sonication, stabilization, and composite properties. *Polymers*. 2012;4(1):275-295.
32. Kharissova OV, Kharisov BI, de Casas Ortiz EG. Dispersion of carbon nanotubes in water and non-aqueous solvents. *RSC Adv*. 2013;3(47):24812-24852.
33. Chen Y, Wang Y, Wang Z, et al. Densification by compaction as an effective low-cost method to attain a high areal lithium storage capacity in a CNT@Co_3O_4 sponge. *Adv Energy Mater*. 2018;8(19):1702981.
34. Grzechnik A, Vegas A, Syassen K, Loa I, Hanfland M, Jansen M. Reversible antifluorite to anticotunnite phase transition in Li_2S at high pressures. *J Solid State Chem*. 2000;154(2):603-611.
35. Cai K, Song M-K, Cairns EJ, Zhang Y. Nanostructured Li_2S–C composites as cathode material for high-energy lithium/sulfur batteries. *Nano Lett*. 2012;12(12):6474-6479.
36. Liang X, Hart C, Pang Q, Garsuch A, Weiss T, Nazar LF. A highly efficient polysulfide mediator for lithium–sulfur batteries. *Nat Commun*. 2015;6:5682.
37. Liang X, Kwok CY, Lodi-Marzano F, et al. Tuning transition metal oxide-sulfur interactions for long life lithium sulfur batteries: the "goldilocks" principle. *Adv Energy Mater*. 2016;6(6):1501636.
38. Ming J, Cao Z, Wahyudi W, et al. New insights on graphite anode stability in rechargeable batteries: Li ion coordination structures prevail over solid electrolyte interphases. *ACS Energy Lett*. 2018;3(2):335-340.
39. Nanda S, Bhargav A, Jiang Z, Zhao X, Liu Y, Manthiram A. Implications of in situ chalcogen substitutions in polysulfides for rechargeable batteries. *Energy Environ Sci*. 2021;14(10):5423-5432.
40. Ye F, Noh H, Lee H, Kim H-T. Ultrahigh capacity graphite/Li_2S battery with Holey-Li_2S nanoarchitectures. *Adv Sci*. 2018;5(7):1800139.
41. Seita T, Matsumae Y, Liu J, et al. Graphite–lithium sulfide battery with a single-phase sparingly solvating electrolyte. *ACS Energy Lett*. 2020;5(1):1-7.
42. Zhu W, Paolella A, Kim C-S, et al. Investigation of the reaction mechanism of lithium sulfur batteries in different electrolyte systems by in situ Raman spectroscopy and in situ X-ray diffraction. *Sustainable Energy Fuels*. 2017;1(4):737-747.
43. Yang C, Suo L, Borodin O, et al. Unique aqueous Li-ion/sulfur chemistry with high energy density and reversibility. *Proc Natl Acad Sci USA*. 2017;114(24):6197-6202.
44. Seh ZW, Wang H, Hsu P-C, et al. Facile synthesis of Li_2S–polypyrrole composite structures for high-performance Li_2S cathodes. *Energy Environ Sci*. 2014;7(2):672-676.
45. Daly FP, Brown CW. Raman spectra of sodium tetrasulfide in primary amines. Evidence for sulfide (S_4^{2-} and S_8^{n-}) ions in rhombic sulfur-amine solutions. *J Phys Chem*. 1975;79(4):350-354.
46. Daly FP, Brown CW. Raman spectra of rhombic sulfur dissolved in secondary amine. *J Phys Chem*. 1976;80(5):480-482.
47. Yu S-H, Huang X, Schwarz K, et al. Direct visualization of sulfur cathodes: new insights into Li–S batteries via operando X-ray based methods. *Energy Environ Sci*. 2018;11(1):202-210.
48. Zielke L, Barchasz C, Waluś S, et al. Lithium/sulfur batteries upon cycling: structural modifications and species quantification by in situ and operando X-ray diffraction spectroscopy. *Adv Energy Mater*. 2015;5(16):1500165.

SUPPORTING INFORMATION

Additional supporting information can be found online in the Supporting Information section at the end of this article.

How to cite this article: Kim H, Min K-J, Bang S, et al. Long-lasting, reinforced electrical networking in a high-loading Li_2S cathode for high-performance lithium–sulfur batteries. *Carbon Energy*. 2023;1-14. doi:10.1002/cey2.308